communications biology

A Nature Portfolio journal

Article

https://doi.org/10.1038/s42003-025-09201-6

TRIM21 promotes K63-linked ubiquitination of ALKBH5 and suppresses cuproptosis via down-regulation of LIAS in esophageal squamous cell carcinoma

Check for updates

Anqi Feng[1,3], Lingnan He[1,3], Zhaoxing Li[1,3], Zeyu Wang[1], Mingchuang Sun[1], Ziying Zhao[1], Zehua Zhang[1], Kang Fang[1], Hao Wu[1], Xiaoyuan Wang[1], Shihan Zhang[1], Zhukai Chen[1], Li Zhang[2], Tao Chen[1] ✉ & Meidong Xu[1] ✉

Cuproptosis is a newly discovered programmed cell death regulated by lipoic acid synthase (LIAS) in cancer cells. However, its functions in Esophageal squamous cell carcinoma (ESCC) and the underlying mechanism remains unclear. Here, we show that in human ESCC cells, TRIM21 facilitates the K63-linked ubiquitination dependent translocation of ALKBH5 from cytosol to nucleus and augments its m6A demethylase activity. LIAS mRNA was demethylated by ALKBH5, and then further identified by reader IGF2BP3, which comprehensively caused the lower expression of LIAS. Moreover, O-GlcNAc transferase OGT facilitated TRIM21-mediated K63-ubiquitination of ALKBH5. Combined treatment with an OGT inhibitor OSMI-1 and copper ionophore elesclomol eliminates tumor growth and remarkably enhances the sensitivity of tumor cells to cisplatin. Together, our study identifies TRIM21 Ubiquitinated-ALKBH5 as a critical gatekeeper to restrict cuproptosis, and such mechanism may contribute to tumor development and drug resistance in ESCC.

Esophageal Squamous Cell Carcinoma is a lethal malignancy. According to the latest cancer statistics released by the World Health Organization's International Agency for Research on Cancer show that in 2020, there were over 600,000 new cases of esophageal cancer worldwide, with 544,000 deaths[1]. The pathological types of esophageal cancer mainly include squamous cell carcinoma (ESCC) and adenocarcinoma[2]. Among the newly diagnosed cases of esophageal cancer worldwide, squamous cell carcinoma accounts for over 85%. More than half of the new cases and deaths of esophageal cancer occur in China, with esophageal squamous cell carcinoma (ESCC) being the main type[1]. The overall prognosis of ESCC is still poor, with a 5-year survival rate of only 15–25%[3]. Tumor progression and metastasis are the primary reasons for treatment failure in ESCC[4]. Given this, we explored the potential role of cuprotosis in ESCC through the analysis of clinical samples combined with database information and found that the key gene LIAS and cuprotosis it mediates may be closely related to the development and prognosis of ESCC.

Abnormal expression of E3 ligases has been known to regulate the activity of oncogenes and tumor suppressors, thereby influencing tumor cell growth, invasion, and metastasis, playing a significant role in tumor progression[5]. The tripartite motif (TRIM) family is a crucial member of the ubiquitin ligase family, and TRIM family molecules are characterized by three structural domains: a RING finger domain at the N-terminus, one or two zinc-binding B-box sequences, and a coiled-coil domain at the C-terminus[6]. Over 70 members of the TRIM family have been discovered, and most of them possess E3 ubiquitin ligase activity, participating in various biological processes such as cell differentiation, growth, proliferation, and apoptosis[7]. RNA N6-methyladenosine (m6A) methylation is the most abundant modification found on mRNA, primarily occurring in the coding sequence (CDS) and 3' untranslated region (3'UTR) of mRNA. This modification affects mRNA stability, translation efficiency, alternative splicing, and cellular localization[8]. Previous studies have shown that the different distributions of m6A methylation on RNA play crucial regulatory roles in tumor malignancy progression[9–11]. ALKBH5 is a widely distributed RNA demethylase present within tumor cells. It specifically removes m6A methylation, thereby modulating mRNA stablization and DNA repair capacity[12]. Together with RNA methyltransferases, ALKBH5 is responsible

[1]Endoscopy Center, Department of Gastroenterology, Shanghai East Hospital, School of Medicine, Tongji University, Shanghai, 200120, China. [2]Department of Pathology, Shanghai East Hospital, School of Medicine, Tongji University, Shanghai, 200120, China. [3]These authors contributed equally: Anqi Feng, Lingnan He, Zhaoxing Li. ✉e-mail: chentao@tongji.edu.cn; 1800512@tongji.edu.cn

for regulating the balance of RNA methylation[13]. This study uncovered that ALKBH5 undergoes ubiquitination modification by TRIM21, subsequently facilitating its nuclear translocation, and thereby regulates cuproptosis through controlling LIAS expression. LIAS is an important enzyme in the human body that synthesizes lipoic acid and in critical biological processes like protein synthesis and carbohydrate metabolism[14], it is now reported to play essential roles in cuproptosis. Cuprotosis is a unique form of cell death which was recently discovered, it differs from other regulated cell death (RCD) in that it involves the accumulation of copper in mitochondria which drives the aggregation of lipidated TCA cycle enzymes[15], leading to oxidative stress and cytotoxicity[16]. This process is regulated by lipoic acid synthase (LIAS) and ferredoxin 1 (FDX1)[17]. A multitude of copper-bearing molecules can attach to copper ions, aiding in the transportation of copper. One standout example is elesclomol (ES), which demonstrates an exceptional efficiency and specificity in directly transporting Cu2+ into mitochondria, making it especially intriguing[18,19]. Nevertheless, its clinical application has faced scrutiny because ES is rapidly metabolized in circulation, leading to a brief half-life and inadequate tumor accumulation. In this study, we enhanced the therapeutic efficacy of elesclomol (ES) by targeting molecular pathways to increase tumor cell sensitivity to ES, thereby potentially holding significance for clinical implications.

Altogether, E3 ubiquitin ligase TRIM21 increases the nuclear entry of ALKBH5 through K63-ubiquitination modification, and this process is regulated by the glycosylation of OGT; nuclear ALKBH5-mediated LIAS mRNA demethylation affects its stability, downregulates LIAS expression, and inhibits cuproptosis in esophageal cancer cells. And through targeted inhibition, we enhanced ES efficiency and promoted it cooperative effect with cisplatin.

Results

TRIM21 is negatively correlated with the clinical outcomes of patients with ESCC

Through the analysis of the expression profiles of TRIM family in TCGA-ESCA database, we found that TRIM21 is one of the most significantly differentially expressed genes between esophageal cancer and normal tissues (Fig. 1A), Through the analysis in the TCGA database, it was found that that TRIM21 was overexpressed in Cholangio carcinoma, Esophageal carcinoma, Glioblastoma and Head and Neck squamous cell carcinoma (Fig. 1B). A Gene Ontology (GO) analysis of genes correlated with TRIM21 indicated enrichment in functions related to Cellular response to chemical stress, Apoptosis, Glycosyltransferase activity, and RNA-binding (Fig. 1C). TRIM21 expression profiles based on histology type was screened out and the expression of TRIM21 was significantly higher in ESCC compared with normal tissues (Fig. S1A). Subsequently, the expression levels of TRIM21 in tumors and normal tissues were assessed using quantitative real-time PCR (qRT-PCR) and Western Blot (Fig. S1B, C). Our results consistently showed that the levels of TRIM21 were markedly elevated in esophageal squamous cell carcinoma (ESCC) tissue samples compared to their corresponding normal tissue counterparts. Immunohistochemical staining of peritumoral tissues and ESCC tissues at different stages also confirmed the aforementioned results (Fig. S1D–F). Based on TRIM21 expression, patients were divided into TRIM21-high ($n = 57$) and TRIM21-low groups ($n = 41$, cut-off value = 6). The correlation analysis was performed between the progression (Stage I, II, III, IV) and tumor grade (G1, G2, G3), and the results showed that the expression level of TRIM21 is not only negatively correlated with the clinical outcomes of patients with esophageal squamous cell carcinoma (ESCC) (Fig. S1G), but also positively correlated with tumor stage and grade (Fig. S1H). ESCC and epithelial cell lines were also assessed by Western Blot (Fig. S1I) in order to screen out the cell lines (ECA109, KYSE30) that highly express TRIM21.

TRIM21 promotes the K63-ubiquitination of ALKBH5

Given previous research findings of TRIM21's role as an E3 ligase primarily mediating protein ubiquitination, immunoprecipitation of TRIM21 followed by Coomassie blue staining were performed (Fig. 1D). Mass spectrometry analysis revealed that TRIM21 interacts with ALKBH5 (Fig. 1E). Subsequently, co-immunoprecipitation (co-IP) of TRIM21 and ALKBH5 was conducted, with Western blot analysis confirming the interaction between TRIM21 and ALKBH5 (Fig. 1F). In addition, we further confirmed the interaction between TRIM21 and ALKBH5 through the in vitro protein binding assay GST-Pull down, demonstrating that they can interact with each other both in vitro and in vivo (Fig. 1G). Following this, knockdown and overexpression of TRIM21 were performed, and qRT-PCR assays were used to evaluate their impact on ALKBH5 expression (Fig. S1J). The results showed that alterations in TRIM21 expression did not lead to corresponding changes in ALKBH5 expression levels. To further investigate, plasmids overexpressing ALKBH5-Flag, TRIM21-Myc, and HA-UB were transfected into HEK-293T cells. Upon Flag antibody-mediated co-IP, it was evident that overexpression of TRIM21 significantly promoted ALKBH5 ubiquitination (Fig. 1H). Further exploration into K63- and K48-linked ubiquitination revealed that TRIM21 primarily regulates ALKBH5 through K63-linked rather than K48-linked ubiquitination (Fig. 1I). A dose-response analysis with TRIM21 confirmed TRIM21's mediation of ALKBH5's K63-linked ubiquitination (Fig. S1K). The RING domain is a principal functional domain of TRIM21, when truncated, its ability to ubiquitinate ALKBH5 was markedly reduced (Fig. 1J). Based on protein sequences obtained from the PDB database, molecular docking analyses were conducted between TRIM21 and ALKBH5. The results identified the binding sites as mainly situated within the core active center region of ALKBH5 (amino acid positions 66-292) (Fig. 1K). Therefore, we hypothesize that the ubiquitination sites of ALKBH5 are located within the protein's active core domain. Guided by previous literature and Mass spectrometry analysis, we generated ALKBH5 ubiquitination site mutants and identified K147 as the primary ubiquitination site targeted by TRIM21 (Fig. 1L). Mutation of K147 to arginine (K147R) significantly inhibited TRIM21-mediated ubiquitination of ALKBH5 (Fig. 1M). Given that K63 ubiquitination can impact on protein expression, localization, and activity in multiple ways, and considering that the primary site of RNA demethylation by ALKBH5 is within the nucleus, we speculate that TRIM21 modulates the nuclear-cytoplasmic shuttling of ALKBH5. Nuclear and cytoplasmic fractionation assays confirmed this hypothesis, the distribution of the ALKBH5 K147R mutant in the nucleus is reduced compared to the wild type (WT) (Fig. 1N).

ALKBH5 suppresses cuproptosis by regulating m6A demethylation modification on LIAS mRNA

To determine the downstream genes that are regulated by ALKBH5 and to identify genes exhibiting correlation with ALKBH5, an overexpression experiment of ALKBH5 was conducted. Subsequently, potential ALKBH5-regulated genes were filtered out using RNA sequencing. The results showed reduced expression of LIAS and IGF2BP3 following ALKBH5 overexpression (Fig. 2A). Differentially expressed genes (logFC > 1) underwent KEGG pathway, GO and DO analysis, revealing enrichment in pathways such as the TCA cycle, Nucleocytoplasmic Transport, and RNA Degradation (Fig. 2B, Fig. S2A, B). GSEA analysis further confirmed significant correlations between these pathways and ALKBH5 (Fig. 2C, Fig. S2C).

Previous studies have demonstrated that LIAS was downregulated in numerous human malignancies, including gastric cancer[20], triple negative breast cancer[21], and head and neck squamous cell carcinoma[22]. According to gene expression profiles through TCGA, we found that LIAS was downregulated in ovarian cancer, esophageal carcinoma and upregulated in Diffuse Large B-cell Lymphoma, Lower Grade Glioma and Thymoma (Fig. S3A, B). Notably, in the TMA consisting of 100 paired ESCC tissue samples, patients were divided into LIAS-high ($n = 51$) and LIAS-low groups ($n = 43$, cut-off value = 6). Kaplan–Meier survival analysis showed that LIAS-low patients had poorer clinical outcomes than LIAS-high patients (logrank $P = 0.0086$) (Fig. S3C). Then, LIAS expression were examined through Western Blot, qRT-PCR and IHC, we consistently detected significantly lower expression levels of LIAS in ESCC tissue samples or cell lines than in paired normal ones (Fig. S3D–H). The correlation

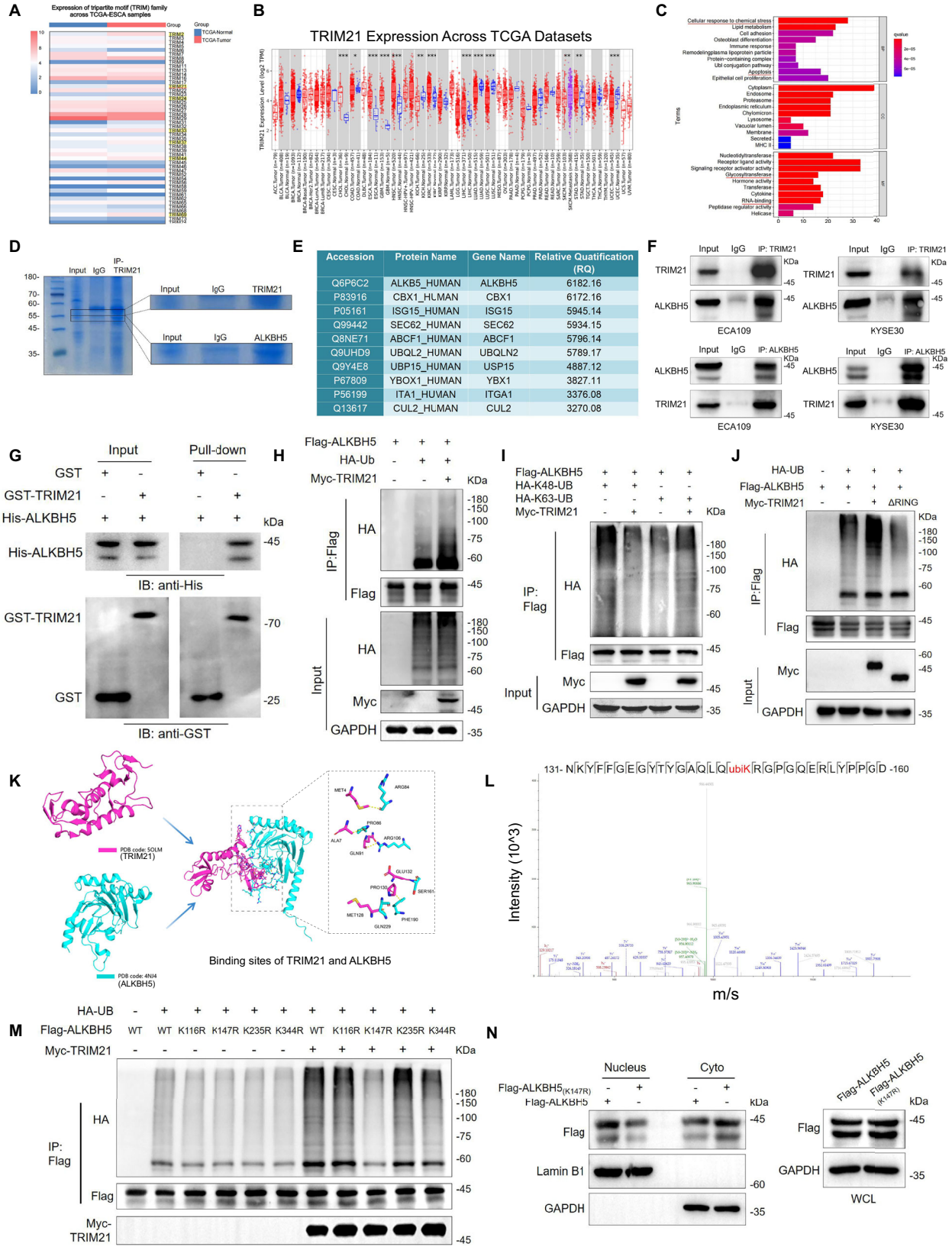

analysis was performed between the progression and tumor grade, and the results showed that LIAS is negatively correlated with tumor stage and grade (Fig. S3I, J). Furthermore, CCK8 and flow cytometry were used to detect the effect of LIAS knockdown on the sensitivity of tumor cells to cuproptosis. We found that down-regulation of LIAS reduced the sensitivity of tumor cells to the copper carrier Elesclomol (Fig. S3K, L). These findings demonstrate that LIAS is a key dysregulated molecule determining the sensitivity to cuproptosis in ESCC. In order to further clarify the regulatory relationship between ALKBH5 and LIAS, RNA Immunoprecipitation (RIP) of ALKBH5 was performed, qRT-PCR and PCR results both indicated a

Fig. 1 | TRIM21 promotes the K63-ubiquitination of ALKBH5. A Expression of Tripartite Motif Containing family across TCGA-ESCA datasets. **B** Expression profiles of TRIM21 across TCGA datasets. **C** GO enrichment analysis of TRIM21 correlated genes. **D** Immunoprecipitation of TRIM21 followed by Coomassie blue staining. **E** Partial mass spectrometry results following TRIM21 co-immunoprecipitation (co-ip). **F** Co-immunoprecipitation (co-IP) followed by western blot analysis of TRIM21 and ALKBH5. **G** GST-Pull down of indicated proteins, demonstrating the molecular binding of TRIM21 and ALKBH5 in vitro. **H** Plasmids overexpressing ALKBH5-Flag, TRIM21-Myc, and HA-UB were transfected into HEK-293T cells and ubiquitination modification was detected by Western Blot. **I** Transfection of K63- and K48-linked ubiquitination and indicated plasmids followed by Western Blot analysis. **J** Transfection of plasmids over-expressing truncated RING domain of TRIM21 and indicated plasmids followed by Western Blot analysis. **K** Molecular docking and predicted binding sites of TRIM21 and ALKBH5 based on protein sequences obtained from the PDB database. **L** Mass spectrometry analysis suggests that the ubiquitination site of ALKBH5 may be located at K147. **M** Transfection of plasmids overexpressing ALKBH5 ubiquitination site mutants and indicated plasmids followed by Western Blot analysis. **N** Nuclear and cytoplasmic fractionation followed by Western blot analysis showing mutation of ALKBH5's K147 ubiquitination site suppressed ALKBH5 translocation to the nucleus (ns: none significant; $^{*}p < 0.05$; $^{**}p < 0.01$; $^{***}p < 0.001$).

significant binding of ALKBH5 to LIAS mRNA (Fig. 2D, E). Actinomycin D was then used to inhibit RNA synthesis, and qRT-PCR assays for RNA stability showed that knocking down TRIM21 or ALKBH5 significantly increased LIAS mRNA stability (Fig. 2F, G). Measurement of m6A modification levels on LIAS through m6A-IP demonstrated reduced m6A methylation on LIAS mRNA upon overexpression of TRIM21 or ALKBH5, whereas m6A modification was significantly enhanced when TRIM21 and ALKBH5 were knocked down (Fig. 2H, I). RIP-qPCR for IGF2BP3 revealed binding of LIAS mRNA to IGF2BP3 (Fig. 2J). Knocking down IGF2BP3 notably decreased both the RNA and protein expression levels of LIAS, and this effect was partially rescued by concurrent knockdown of ALKBH5 (Fig. 2K, L). Moreover, LIAS mRNA stability was also significantly reduced after IGF2BP3 knockdown (Fig. 2M), suggesting that ALKBH5-mediated RNA demethylation of LIAS is recognized by IGF2BP3, leading to decreased mRNA stability and subsequent reduction in mRNA expression levels.

TRIM21-mediated-K63 ubiquitination of ALKBH5 promotes it nucleus localization and suppresses cuproptosis

To validate TRIM21's regulatory effect on LIAS, TRIM21 was knocked down, and the efficiency of the knockdown was assessed by qRT-PCR and western blot (Fig. S4A, B). Although there is no binding relationship between TRIM21 and LIAS (Fig. S4C). Knockdown or overexpression of TRIM21 exerted a significant negative regulatory effect on the protein expression of LIAS (Figs. 3A, S4D, E), suggesting a suppressive role of TRIM21 on LIAS. To further explain the mechanism, Nuclear and cytoplasmic fractionation assays were performed and reduced nuclear distribution of ALKBH5 upon TRIM21 knockdown was detected (Fig. 3B). We further validated this mechanism through immunofluorescence staining (IF), demonstrating that TRIM21 modulates LIAS expression by regulating the nucleocytoplasmic trafficking of ALKBH5 (Fig. 3C) and mutation of ALKBH5's ubiquitination site K147 also impeded its nuclear translocation (Fig. S4F). Moreover, similar to ALKBH5 knockdown, mutation of ALKBH5's ubiquitination site had a pronounced upregulation on LIAS expression (Fig. S4G, H). Moving forward to functional validation, IC50 of tumor cells to the copper carrier Elesclomol and Cu2+ complex in ESCC cell lines ECA109 and KYSE30 were examined (Fig. S4I). The results from CCK8 assays demonstrated that knockdown of TRIM21 by lentivirus or ALKBH5 by siRNA decreased ESCC cell proliferation (Fig. S5A, B). In apoptosis experiments, flow cytometry demonstrated that knockdown of TRIM21 or ALKBH5 both increased the sensitivity of cells to cuproptosis. However, simultaneous knockout of LIAS attenuated or even counteracted this effect (Fig. 3D). In line with this, knockdown of TRIM21 or ALKBH5 inhibited the viability of tumor cells under copper carrier stimulation, and this effect could also be reversed by LIAS knockdown (Fig. 3E, Fig. S5C). In addition, by measuring the mitochondrial copper ion concentration in cells, we found that knockdown of TRIM21 increased the copper ion concentration in mitochondria under Elesclomol-Cu^{2+} stimulation (Fig. S5D). Since LIAS aggregation may lead to changes in mitochondrial membrane permeability during copper-induced cell death, allowing cytoplasmic copper ions to more easily enter the mitochondria, knockdown of LIAS also restored this phenomenon (Fig. S5D). These results indicate that LIAS is a direct target gene of TRIM21/ALKBH5 axis and plays a specific and crucial role in modulating the sensitivity to cuproptosis. Similarly, overexpression of ALKBH5-K147R mutant, compared with ALKBH5-WT, also significantly enhanced sensitivity to cuproptosis (Fig. 3F). These findings collectively point to a critical role for TRIM21 in regulating ALKBH5 localization, which in turn affects LIAS expression and cuproptosis sensitivity in ESCC cells.

TRIM21 suppresses LIAS expression and cuproptosis in xenograft tumor models

To further investigate the impact of TRIM21 on LIAS in vivo and its influence in sensitivity to elesclomol-induced cuproptosis, we established a subcutaneous xenograft tumor model in nude mice using the esophageal squamous cell carcinoma cell line ECA109. Mice were injected with elesclomol in both control (Ctrl) and TRIM21 knockdown (shTRIM21) groups. Tumor sizes and weights are depicted in the figures (Fig. 4A, B). Proteins and RNA from the tumor tissues were extracted for Western Blot analysis, which revealed increased protein and RNA expression levels of LIAS in the shTRIM21 group (Fig. 4C, D). In addition, immunostaining for TRIM21, Ki-67, and TUNEL was performed across the groups, demonstrating that TRIM21 knockdown promoted tumor apoptosis and cuproptosis, while significantly reducing proliferative capacity (Fig. 4E, F).

TRIM21-mediated-K63 ubiquitination of ALKBH5 is regulated by the O-GlcNAc transferase OGT

Previous studies have reported that the RNA demethylase activity of ALKBH5 is influenced by its subcellular localization, and the nuclear-cytoplasmic distribution of ALKBH5 is regulated by O-glycosylation[23]. It is known that protein O-glycosylation is specifically controlled by the O-glycosyltransferase enzyme OGT[24]. Consequently, we further examined the interactions between ALKBH5 and OGT through co-immunoprecipitation assays, revealing that OGT and ALKBH5 interacts with each other (Fig. 5A), suggesting a potential interplay. Furthermore, when Myc-OGT plasmid, along with HA-UB and Flag-ALKBH5, was transfected into HEK-293T cells, overexpression of myc-OGT promoted the ubiquitination of ALKBH5 (Fig. 5B). In addition, co-transfection of TRIM21 with OGT augmented ALKBH5 ubiquitination (Fig. 5C), and overexpression of OGT led to an increase in O-glycosylation of ALKBH5 (Fig. 5D), and knockdown of OGT significantly inhibited the binding of ALKBH5 to TRIM21 (Fig. 5E). Similarly to TRIM21, OGT facilitated K63-linked ubiquitination of ALKBH5 rather than K48-linked ubiquitination (Fig. S6A). Then, OGT was knocked down and reduced ALKBH5 nuclear localization was observed (Fig. S6B). The 147 R mutant also resulted in reduced OGT-mediated ubiquitination (Fig. S6C). Moreover, upon introducing the OGT inhibitor OSMI-1 (Fig. S6D)[25], it was discovered that OSMI-1 not only inhibited ALKBH5 O-glycosylation but also hindered the interaction between TRIM21 and ALKBH5, subsequently suppressing ALKBH5 ubiquitination (Fig. 5F). To comprehensively analyze the roles of TRIM21 and OGT in regulating lipoylated protein aggregation, TRIM21 and OGT were individually knocked down or overexpressed, the results indicated a significant negative correlation between the co-expression of OGT and TRIM21 with LIAS, Lipoylated-DLAT (Lip-DLAT), and

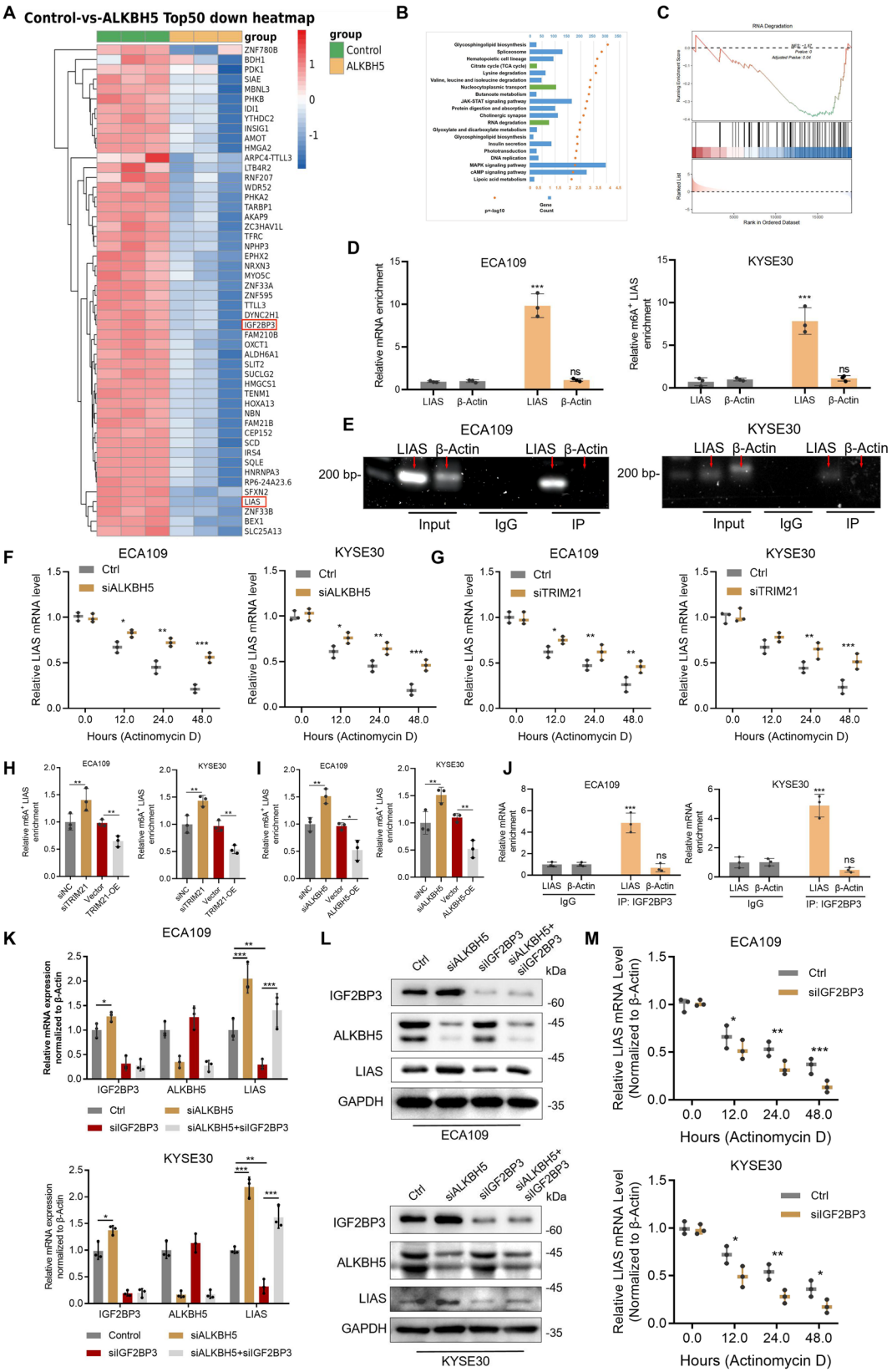

Lipoylated-DLST (Lip-DLST). However, upon OSMI-1 treatment, the expression of Lip-DLAT, Lip-DLST, and LIAS were restored (Fig. 5G, H). Furthermore, with increasing concentrations of OSMI-1, there was a corresponding increase in LIAS and downstream metabolic gene expressions, with a more pronounced rise observed after TRIM21 knockdown (Fig. S6E). Lastly, following treatment with a gradient of OSMI-1 concentrations, nuclear-cytoplasmic fractionation experiments showed that OSMI-1 inhibited ALKBH5's accumulation in the nucleus (Fig. 5I), providing further evidence of OGT's regulatory impact on ALKBH5 localization and function.

Fig. 2 | ALKBH5 suppresses LIAS expression through m6A demethylation modification on LIAS mRNA. **A** Heat map illustrating genes downregulated upon ALKBH5 overexpression detected by RNA sequencing. **B** KEGG pathway analysis of differentially expressed genes (logFC > 1). **C** GSEA analysis confirmed significant correlations between RNA degradation pathways and ALKBH5 expression. **D** RNA Immunoprecipitation (RIP) of ALKBH5 followed by qRT-PCR ($n = 3$ independent experiments). **E** RNA Immunoprecipitation (RIP) of ALKBH5 followed by PCR. **F** qRT-PCR assays for RNA stability showed that knocking down TRIM21 increased LIAS mRNA stability ($n = 3$ independent experiments). **G** qRT-PCR assays for RNA stability showed that knocking down ALKBH5 increased LIAS mRNA stability ($n = 3$ independent experiments). **H** Measurement of m6A modification levels on LIAS through m6A-IP after knocking down or overexpression of TRIM21 ($n = 3$ independent experiments). **I** Measurement of m6A modification levels on LIAS through m6A-IP after knocking down or overexpression of ALKBH5 ($n = 3$ independent experiments). **J** RIP-qPCR for IGF2BP3 revealed binding of LIAS mRNA to IGF2BP3 ($n = 3$ independent experiments). **K** Knocking down IGF2BP3 notably decreased both the RNA expression levels of LIAS, and this effect was partially rescued by concurrent knockdown of ALKBH5 ($n = 3$ independent experiments). **L** Knocking down IGF2BP3 notably decreased both the protein levels of LIAS, and this effect was partially rescued by concurrent knockdown of ALKBH5 ($n = 3$ independent experiments). **M** qRT-PCR showed LIAS mRNA stability was reduced after IGF2BP3 knockdown ($n = 3$ independent experiments). Error bars indicate standard deviations (ns: none significant; $^{*}p < 0.05$; $^{**}p < 0.01$; $^{***}p < 0.001$).

Combined application of Elesclomol and OSMI-1 significantly eliminates tumor growth and remarkably enhances the sensitivity of tumor cells to cisplatin

To further validate the synergistic effect between OSMI-1 and Elesclomol, flow cytometry was employed to assess cell apoptosis after treatment with OSMI-1 in conjunction with Elesclomol-Cu^{2+}. The results demonstrated that OSMI-1 significantly enhanced cellular susceptibility to cuproptosis (Fig. 6A). Meanwhile, the detection of mitochondrial copper ion concentration showed that OSMI-1 could increase the copper ion concentration in cellular mitochondria under ES-Cu2+ stimulation (Fig. 6B). Likewise, reactive oxygen species (ROS) detection revealed that OSMI-1 notably shifted the absorption peak to the right under Elesclomol-Cu^{2+} stimulation (Fig. 6C). The morphological changes of ECA109 cells under different drug treatments were captured under a bright-field microscope (Fig. 6D). 3D cell culture and staining with Hoechst and PI showed that there was a significant cell death in the 3D culture system when OSMI-1 and ES were combined (Fig. 6E). Furthermore, subcutaneous xenograft tumors in nude mice were established, with OSMI-1 or Elesclomol administered intraperitoneally. Tumor growth was slowest when both drugs were combined (Fig. 6F–H). Immunohistochemical staining indicated the lowest Ki-67 scores and highest TUNEL scores in the combination therapy group (Fig. 6I, J).

Previous studies have reported that Elesclomol enhances the sensitivity of cisplatin-resistant tumor cells to cisplatin[26]. Therefore, we further explored the sensitizing effects of OSMI-1 and Elesclomol on cisplatin. Cell viability assays (CCK8) revealed near-complete inhibition of cell activity with the triple combination of OSMI-1, Elesclomol-Cu^{2+}, and cisplatin (Fig. 7A, B). 3D cell culture experiments showed that the combination of OSMI-1 and ES could significantly reduce or even eliminate 3D cell spheroids when combined with cisplatin (Fig. 7C). In the in vivo experiment, the subcutaneous xenograft tumor model in nude mice confirmed this finding, where Elesclomol significantly inhibited tumor growth, and co-administration with OSMI-1 led to tumor stasis or reduction (Fig. 7D–F). Immunohistochemistry (IHC) further substantiated that the triple therapy with OSMI-1, Elesclomol-Cu^{2+}, and cisplatin resulted in extensive necrotic areas within the tumor tissue, increased immune cell infiltration, diminished Ki-67 staining, and a marked TUNEL staining increase (Fig. 7G, H).

Discussion

E3 ligase TRIM21 has previously been reported to be negatively associated with the prognosis of various tumors[27–30]. It has been revealed that TRIM21 not only controls ubiquitin-mediated lysosomal degradation process in tumor cells such as ApoE in hepatocellular carcinoma[29] and autophagic degradation of c-Myc in colorectal cancer[30], but also regulates protein activity such as MST2 through K63 ubiquitination modification[31]. Our study confirms that TRIM21 is aberrantly overexpressed in esophageal cancer, particularly in esophageal squamous cell carcinoma (ESCC), compared to other members of the TRIM family. Moreover, its expression is negatively correlated with the prognosis of patients with ESCC. Mechanistically, we uncover an interaction between TRIM21 and ALKBH5, the latter being a well-established RNA demethylase[32], which influences RNA stability and gene expression of LIAS as we have found. LIAS is an essential gene regulating cuproptosis[33]. Cuprotosis differs from other RCDs in that it involves the accumulation of copper iron, which is closely related to the process of protein lipidation and the tricarboxylic acid (TCA) cycle[34]. This process is mainly regulated by lipoic acid synthase (LIAS) and ferredoxin 1 (FDX1)[33]. Although research on copper in drug development suggests a certain prospect in anticancer therapy[35], little is known about its molecular regulating mechanisms and role of chemotherapy resistance[36]. There is an urgent need to identify key molecules from appropriate patient populations and delve deeper into their molecular mechanisms[37].

Previous studies have shown that ALKBH5 can be post-transcriptional modified such as ubiquitination[38], SUMOylation[39] or phosphorylation[39], thereby influencing their stability or enzymatic activity, but no studies have reported ALKBH5 undergoing K63 ubiquitination that could affect its subcellular localization. In this study, we uncover that TRIM21 regulates ALKBH5 demethylase activity by modulating its nuclear translocation. We then further identified how TRIM21 regulates cuproptosis through ALKBH5. Experimental validation showed that TRIM21 mediates K63 ubiquitination modification of ALKBH5. Compared with other types of ubiquitination modifications, K63 ubiquitination has unique biological characteristics and functions and plays an important role in protein localization[40]. Therefore, we speculate that K63 ubiquitination mediated by TRIM21 may be one of the key factors promoting the nuclear entry of ALKBH5 to exert its demethylation function. These results indicate that the TRIM21/ALKBH5 axis may serve as a crucial regulatory factor for LIAS and LIAS-mediated cuproptosis.

To further investigate the possible influencing factors of ALKBH5 nuclear entry, we found that in addition to TRIM21 with E3 ubiquitin ligase function, O-GlcNAc transferase (OGT) is also one of the binding proteins of ALKBH5. O-GlcNAc has been reported to be responsible for nuclear localization of ALKBH5 and the RNA demethylase activity[23]. Our study is consistent with previous findings and further enriches the understanding of the mechanisms behind this phenomenon. Our discovery suggests that in addition to ubiquitination, there may also be O-glycosylation modification catalyzed by OGT in the post-translational modification of ALKBH5. As previously reported, O-glycosylation facilitates K63 ubiquitination by promoting protein interactions[41]. Our findings validated that OGT-mediated O-glycosylation enhances the interaction between ALKBH5 and TRIM21, subsequently promoting K63 ubiquitination of ALKBH5. Furthermore, OSMI-1, a specific inhibitor of OGT[42], effectively suppressed protein O-glycosylation, as well as K63-ubiquitination and nuclear translocation of ALKBH5, consequently suppressing its demethylase activity.

As mentioned in earlier studies, cuproptosis inducers hold great potential as key targets for addressing chemoresistance in tumor therapy[43]. Our study demonstrates the chemosensitizing effect of cuproptosis inducer by combining Elesclomol with cisplatin, and further confirms the synergistic promotion of copper-mediated cell death and chemotherapeutic agents through the additional employment of glycosidase inhibitors, thereby targeting this pathway.

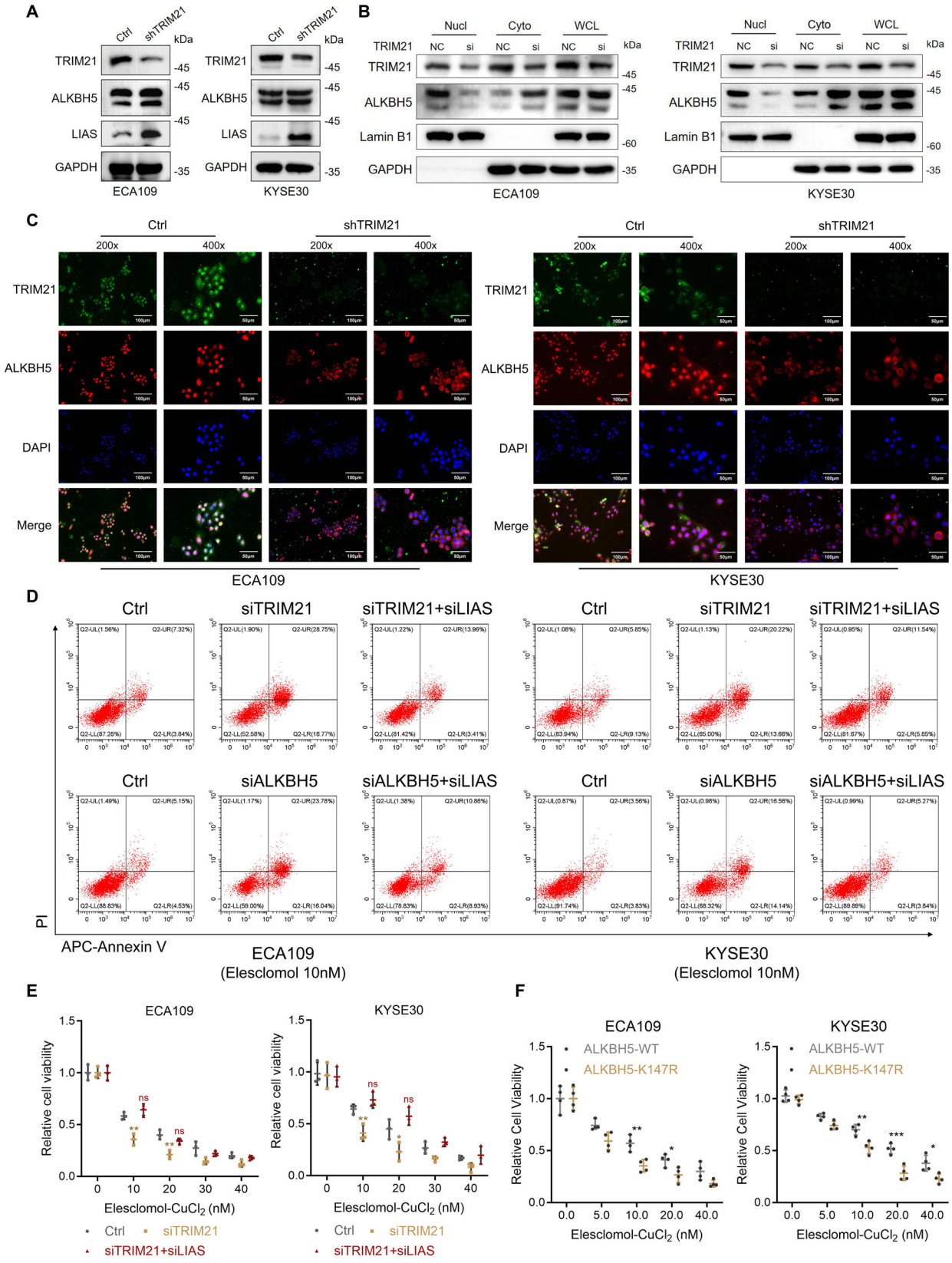

Conclusions

In conclusion, this study confirms the regulatory pathway mediated by TRIM21, ALKBH5, IGF2BP3, and LIAS in controlling cuproptosis, and further demonstrates the pivotal role of the glycosyltransferase OGT as well as the promoting effect of the glycosylation enzyme inhibitor OSMI-1 on cuproptosis and its sensitizing effect on Cisplatin. This regulatory mechanism provides new insights into the understanding of Cuproptosis and may open new avenues for the development of therapeutic strategies targeting Cuproptosis in esophageal squamous cell carcinoma (ESCC) and other malignancies.

Fig. 3 | TRIM21 promotes ALKBH5 nucleus localization and suppresses cuproptosis. A Western blot showing knockdown of TRIM21 significantly increased LIAS expression without affecting ALKBH5 expression. **B** Nuclear and cytoplasmic fractionation assays followed by Western Blot analysis showed decreased ALKBH5 nuclear localization upon TRIM21 knockdown. **C** Immunofluorescence staining (IF) demonstrating that knockdown of TRIM21 supresses the nucleocytoplasmic trafficking of ALKBH5. **D** Apoptosis experiments illustrated that ESCC cells knockdown of TRIM21 or ALKBH5 both increased the sensitivity of cells to cuproptosis, while simultaneous knockout of LIAS attenuated or even counteracted this effect. **E** CCK8 assays showing that knockdown of TRIM21 inhibited the viability of tumor cells under elesclomol-Cu^{2+} stimulation, and this effect could be reversed by LIAS knockdown ($n = 3$ independent experiments). **F** CCK8 assays showing that ESCC cells became more susceptible to elesclomol-Cu^{2+}-induced cuproptosis after mutation on ubiquitination site K147 (K147R) compared to Wild Type (WT) ($n = 3$ independent experiments). Error bars indicate standard deviations (ns: none significant; $^{*}p < 0.05$; $^{**}p < 0.01$; $^{***}p < 0.001$).

Methods

Data collection

The Cancer Genome Atlas (TCGA, https://www.cancer.gov/ccg/research/genome-sequencing/tcga) is a large-scale cancer genomics program, and it has molecularly characterized 33 primary cancer types including ESCA. The expression of TRIM21 in ESCA was investigated in Ualcan Website (https://ualcan.path.uab.edu/analysis.html) based on TCGA database. The expression of TRIM21 in pan-cancer was analysed in TIMER2.0 Website (https://compbio.cn/timer2/) based on TCGA database. The expression of LIAS in ESCA and pan-cancer was analysed in Gepia website (http://gepia.cancer-pku.cn/detail.php?gene=LIAS) based on TCGA database.

Functional enrichment analysis

Gene Ontology and KEGG signaling pathway enrichment analyses was carried out and plotted according to the DAVID website (https://david.ncifcrf.gov).

Cell lines and incubation

The human esophageal epithelial cell line Het-1A was purchased from ATCC. The human ESCC cell lines KYSE150, TE-1, KYSE30, ECA109, and KYSE410 were purchased from the Institute of Biochemistry and Cell Biology of the Chinese Academy of Sciences. All human cell lines were identified by short tandem repeat analysis, and the results of mycoplasma testing were negative. All human cell lines were cultured with 3 mL DMEM medium containing 10% FBS (Gibco) with 100 U/mL penicillin and streptomycin (Gibco), and incubated at 37 °C and 5% CO_2 in a humidified incubator of 5% CO_2. The 3D cell culturing was in the basis of the instructions of Centuregel (Yeasen, 40183ES).

Clinical specimens

This study was approved by the institutional review board of Shanghai East Hospital, Tongji University. The human clinical sample was obtained from the Endoscopy Center of Shanghai East Hospital. All human samples were obtained with the patients' written informed consent and consent to publish information that identifies individuals has been obtained. The samples were processed with IHC staining for RNA extraction and western blotting. All ethical regulations relevant to human research participants were followed.

Approval of the research protocol by an institutional review board: All procedures followed were in accordance with the ethical standards of the institutional review board of Tongji University School of Medicine with the Declaration of Helsinki 1964 and later versions.

Animal studies

All animal experiments and procedures were approved by the animal care and use committee of Tongji University. We have complied with all relevant ethical regulations for animal use. BALB/c nude mice were purchased from Changzhou Cavens Laboratory Animal Co. Ltd and housed under standard pathogen-free conditions. The first group includes 16 female BALB/c nude mice (6 weeks old). The animals were randomly divided into 4 groups ((four per group): Control group (Ctrl), shTRIM21 group (shTRIM21), elesclomol treatment group, shTRIM21 combined with elesclomol treatment group). A total number of 3×10^6 shTRIM21/Ctrl tumor cells were injected into the right flank of nude mice. Elesclomol (MedChemExpress (MCE), USA) was diluted into 800 μl of DMSO to reach a final concentration of 156.05 mM and diluted into working solution at 10% concentration[44] (the ingredient of the cosolvent contained 40% PEG300, 5% Tween-80 and 45% saline). When the average tumor size of the control group reached approximately 100 mm3, mice were intraperitoneally injected with the dissolved compounds 4 times for 2 weeks (100 μl per time). The second group includes 16 BALB/C with the same conditions presented above. The animals were randomly divided into 4 groups ((four per group): Control group (Ctrl), OSMI-1 group (OSMI-1), elesclomol treatment group (ES), elesclomol combined with OSMI-1 treatment group). 5 mg/kg OSMI-1 was intraperitoneally administered with (MedChemExpress (MCE), USA) twice a week for 2 weeks, while elesclomol was injected with the same method above. The third group includes 20 BALB/C with the same conditions above. Cisplatin (3 mg/kg/2 days)[45] for 2 weeks when tumor reached approximately 100 mm^3. elesclomol or OSMI-1 treatment was performed according to previous steps. Three weeks later, the mice were killed under anesthesia, and the tumor weight and volume were measured and calculated. The maximal tumour measurements for subcutaneous tumors that were permitted by animal care and use committee of Tongji University is 15 mm in diameter and in none of the experiments were these limits exceeded.

Immunohistochemistry and IF

All paraffin-embedded material was sectioned at 4 μm. After dewaxing and hydration, the sections were incubated overnight with Abs against human TRIM21 (12108-1-AP; Proteintech; concentration: 1:500), human LIAS (11577-1-AP; Proteintech; concentration: 1:200), Ki-67 (9129; Cell Signaling Technology; concentration: 1:1000), human ALKBH5 (16837-1-AP; Proteintech; concentration: 1:500), DYKDDDDK Tag (14793; Cell Signaling Technology; concentration: 1:500), Myc-Tag (2278; Cell Signaling Technology; concentration: 1:500). Primary Ab was detected with HRP-conjugated secondary Abs incubated for 8 min. Sections were washed in distilled water, counterstained with hematoxylin, dehydrated, and mounted. The whole tissue section was scored with staining intensity and percentage and the scoring scale was graded as follows: 0, no staining; 1, light brown staining; 2, brown staining; and 3, dark brown staining. The percentage of positive cells was divided into four levels: 1, <5%; 2, 5–30%; 3, 31–60%; and 4, 61–100%. The IHC staining score was calculated as follows: intensity score × percentage score.

For IF, 5% BSA was used as the blocking buffer before incubation with primary Abs. We used DAPI (Invitrogen) to counterstain the tissues before mounting with fluorescent mounting medium (Dako).

Virus construction and infection

To achieve gene knockdown in cells and get stable clones, a lentivirus-based approach was utilized. First, a lentiviral vector by cloning a specific shRNA targeting TRIM21 into a lentiviral plasmid was constructed. Next, the target cells were infected with the concentrated lentivirus in the presence of polybrene (8 μg/mL, Hanbio Technology Co. Ltd) to enhance infection efficiency. After 48 h, the infection efficiency was assessed by observing GFP expression under a fluorescence microscope. To select for stable knockdown clones, puromycin was added to the culture medium at a concentration that was lethal to uninfected cells but non-lethal to infected cells expressing the puromycin resistance gene. Cells were maintained in the presence of

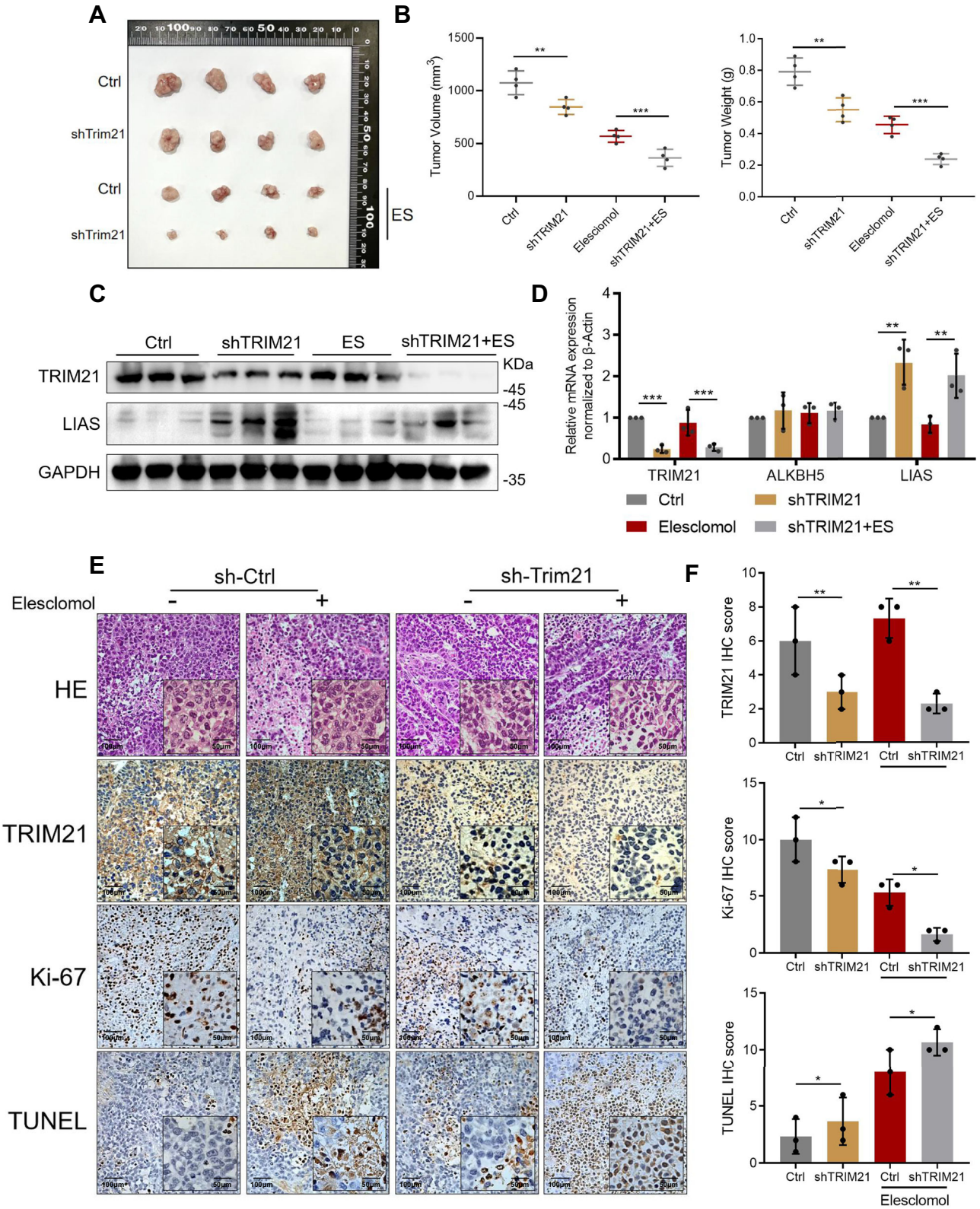

Fig. 4 | TRIM21 suppresses LIAS expression and cuproptosis in xenograft tumor models. A Subcutaneous xenograft tumor model in nude mice using the esophageal squamous cell carcinoma cell line ECA109, mice were injected with elesclomol in both control (Ctrl) and TRIM21 knockdown (shTRIM21) groups. **B** Tumor sizes and weights are depicted in the figure ($n = 4$ independent experiments). **C** Proteins from the tumor tissues were extracted for Western Blot analysis, which revealed TRIM21, LIAS protein expression levels. **D** RNA from the tumor tissues was extracted for qRT-PCR analysis, which revealed TRIM21, LIAS, ALKBH5 mRNA expression levels ($n = 3$ independent experiments). **E** Immunostaining for TRIM21, Ki-67, and TUNEL was performed across the groups. **F** Quantification of (**E**) ($n = 3$ independent experiments). Error bars indicate standard deviations (ns: none significant; $^{*}p < 0.05$; $^{**}p < 0.01$; $^{***}p < 0.001$).

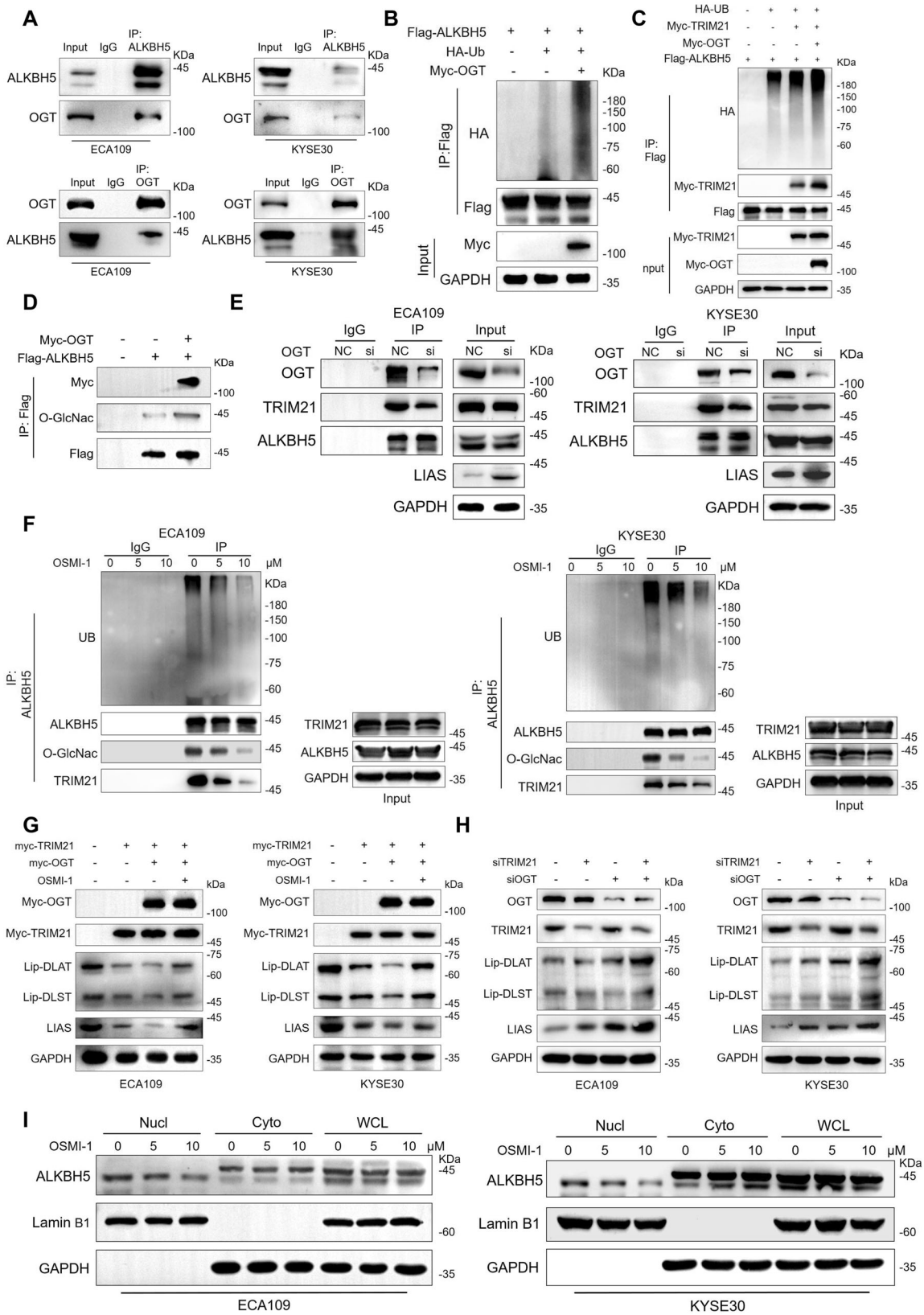

puromycin (Hanbio Technology Co. Ltd) for approximately 2 weeks, during which non-infected cells were eliminated, and stable knockdown clones were enriched. Individual clones were then isolated and further verified for gene knockdown efficiency using qRT-PCR and Western blotting. The shRNA sequences targeting TRIM21 (shTRIM21-1 and shTRIM21-2) and lentivirus for TRIM21 overexpression was designed and constructed by Hanbio Technology Co. Ltd. The shTRIM21 sequences were as follows: GAGTTGGCTGAGAAGTTGGAA (shTRIM21-1) and TGGCATGGTC TCCTTCTACAA (shTRIM21-2).

Fig. 5 | TRIM21-mediated-K63 ubiquitination of ALKBH5 is regulated by the O-GlcNAc transferase OGT. A Co-immunoprecipitation assays revealing that OGT and ALKBH5 can interact with each other. **B** Myc-OGT plasmid, along with HA-UB and Flag-ALKBH5, was transfected into HEK-293T cells, western blot showed overexpression of myc-OGT promoted the ubiquitination of ALKBH5. **C** Western blot showing co-transfection of TRIM21 with OGT augmented ALKBH5 ubiquitination. **D** Co-IP followed by western blot showing overexpression of OGT led to an increase in O-glycosylation of ALKBH5. **E** Co-IP followed by western blot showing knockdown of OGT led to the decrease in the binding of ALKBH5 and TRIM21, also induced upregulation of LIAS. **F** Co-IP followed by western blot analysis showing reduced ALKBH5 O-glycosylation and interaction with TRIM21 upon introducing the OGT inhibitor OSMI-1 in different concentrations. **G** A significant negative correlation in protein expression between the co-expression of OGT and TRIM21 with LIAS, Lipoylated-DLAT (Lip-DLAT), and Lipoylated-DLST (Lip-DLST) expression was observed by western blot, upon OSMI-1 treatment, the expressions of Lip-DLAT, Lip-DLST, and LIAS were restored. **H** Protein expression showing negative correlation between OGT and TRIM21 with LIAS, Lipoylated-DLAT (Lip-DLAT), and Lipoylated-DLST (Lip-DLST) after OGT or TRIM21 knockdown. **I** Following treatment with a gradient of OSMI-1 concentrations, nuclear-cytoplasmic fractionation experiments showed that OSMI-1 inhibited ALKBH5's accumulation in the nucleus.

siRNA sequences targeting ALKBH5, LIAS, OGT was designed and constructed by Hanbio Technology Co. Ltd. siRNA was added to the culture medium of ESCC cells by using riboFECT Transfection Kit (Ribobio, Shanghai, China) as previously described[46]. The siALKBH5 sequences were as follows: CCCATCGTGTCCGTGTCCTTCTTTA (siALKBH5-1) and TGCTTCGGCTGCAAGTTCCAGTTCA (siALKBH5-2). The siLIAS sequences were as follows: GCCTGTAATCCCAGCACTTTA (siLIAS-1) and CGAGGTGATCTCAAAGCAATA (siLIAS-2). The siOGT sequences were as follows: GGCATGTTATTTGAAAGCATT.

RNA extraction and qRT-PCR

Total RNAs were extracted from cells by using TRIzol (Sigma-Aldrich) solution, according to the instructions of the manufacturer, quantified by using Nanodrop 2000 (Thermofisher), and stored at −80 °C. RNA (1000 ng) was reverse transcribed into cDNA using a reverse transcription system (Takara). Real-time qPCR was carried out to quantify the transcripts using SYBR Green PCR Master Mix (Takara). The relative abundance of RNA was normalized to GAPDH. We used $2-(\Delta\Delta Ct)$ to calculate the relative abundance of mRNA. The relevant primers are summarized in Table S1.

Western blot analysis

Cells were lysed in cold RIPA buffer containing protease inhibitors. Equal amounts of total protein were separated by SDS-PAGE (Shanghai Epizyme Biomedical Technology Co., Ltd), transferred to PVDF membranes (Millipore), and blocked in 5% milk. The primary Abs against human LIAS (11577-1-AP; Proteintech; concentration: 1:1000), human TRIM21 (12108-1-AP; Proteintech; concentration: 1:1000), human ALKBH5 (16837-1-AP; Proteintech; concentration: 1:1000), human IGF2BP3 (A23295; Abclonal; concentration: 1:1000), DYKDDDDK Tag (14793; Cell Signaling Technology; concentration: 1:1000), Myc-Tag (2278; Cell Signaling Technology; concentration: 1:1000) and HA-Tag (3724; Cell Signaling Technology; concentration: 1:1000) were diluted according to the instructions. Membranes were incubated overnight with primary Abs at 4 °C, followed by secondary Abs for 1 h at room temperature. Blots were developed using Millipore Immobilon Western Chemiluminescent HRP Substrate. β-Actin and GAPDH were used as loading controls.

Flow cytometry for apoptosis assay

Cells were collected, washed, and treated following instructions of Annexin V-FITC/PI Apoptosis Kit (Elabscience, E-CK-A211). The results were analyzed using the CytExpert 2.4 software program.

In vitro proliferation assay

Cells were seeded in 96-well plates at 1000 cells/well. Cell proliferation was detected using a CCK-8 cell proliferation assay kit at 450 nm following the manufacturer's instructions.

Co-immunoprecipitation

Digest and collect the cultured cells. Use RIPA lysis buffer to mix and lyse the cells for protein extraction. Take 1/10 of the supernatant of the cell lysate as the Input and denature it with SDS. The remaining lysate is used for co-immunoprecipitation experiments. Add 1 μg of IgG antibody to one protein sample as the control group, and add the corresponding primary antibodies to the other protein samples. Incubate overnight at 4 °C on a vertical mixer. After the antibody incubation is complete, take 30 μl of Protein A/G Agarose beads and wash them three times with RIPA lysis buffer. Divide them evenly into the samples mentioned above and incubate them at 4 °C on a vertical mixer for 3 h. Then centrifuge to remove the supernatant and wash the beads with pre-cooled RIPA lysis buffer. Add 1 ml of RIPA each time, gently invert to mix, centrifuge at 3000 r/min at 4 °C for 1 min, and repeat the washing process three times. After the last centrifugation, discard the supernatant, add an appropriate amount of 4xSDS loading buffer, heat at 95 °C for 5–10 min, centrifuge to take the supernatant for subsequent Western Blotting sample loadin or mass spectrometry.

Protein-protein interaction assay (GST Pull-Down)

The GST Pull-Down assay was performed to validate direct protein-protein interactions in vitro. Briefly, the bait protein was expressed as a glutathione S-transferase (GST) fusion protein in E. coli BL21 (DE3) cells and purified using glutathione-Sepharose 4B beads (Cytiva). After pre-equilibration of the beads with lysis buffer (50 mM Tris-HCl pH 8.0, 150 mM NaCl, 1% NP-40, 1 mM EDTA, and protease inhibitors), the purified GST-tagged bait protein (10–20 μg) was bound to the beads by incubation at 4 °C for 2 h with gentle rotation. The prey protein, either as a purified His-tagged protein or in cell lysate, was then added to the bait-bound beads and incubated at 4 °C overnight. Non-specifically bound proteins were removed by washing the beads three times with ice-cold wash buffer (identical to lysis buffer). Protein complexes were eluted using 10 mM reduced glutathione (in 50 mM Tris-HCl, pH 8.0) or directly denatured in 1× SDS loading buffer. Eluted proteins were resolved by SDS-PAGE and interactions were detected via Western blotting using appropriate antibodies against the prey protein. Control experiments with GST alone were included to rule out non-specific binding.

RNA immunoprecipitation

Take an appropriate amount of Protein A + G Agarose and wash it with incubation buffer 2–3 times. Add 500 μl of incubation buffer, 20 μl of Protein A + G Agarose, and 5 μl of anti-N6-methyladenine to a 1.5 ml centrifuge tube. Incubate at 4 °C on a rotary incubator for 3–4 h. Add the fragmented and purified RNA fragments to the centrifuge tube and incubate overnight at 4 °C on the rotary incubator. Centrifuge the sample briefly, discard the supernatant, and wash the Protein A + G Agarose remaining at the bottom of the centrifuge tube with protease K digestion buffer 2–3 times. Add 250 μl of protease K digestion buffer and 5 μl of protease K, and incubate at 95 °C for 5 min. After brief centrifugation, transfer the supernatant to another 1.5 mL centrifuge tube, discard the precipitate, and purify the supernatant to obtain RNA fragments for sequencing.

RNA m6A-RIP qPCR

Total RNA was extracted from cells that had undergone specific treatments, and then treated with DNase (Sigma) to remove genomic DNA.

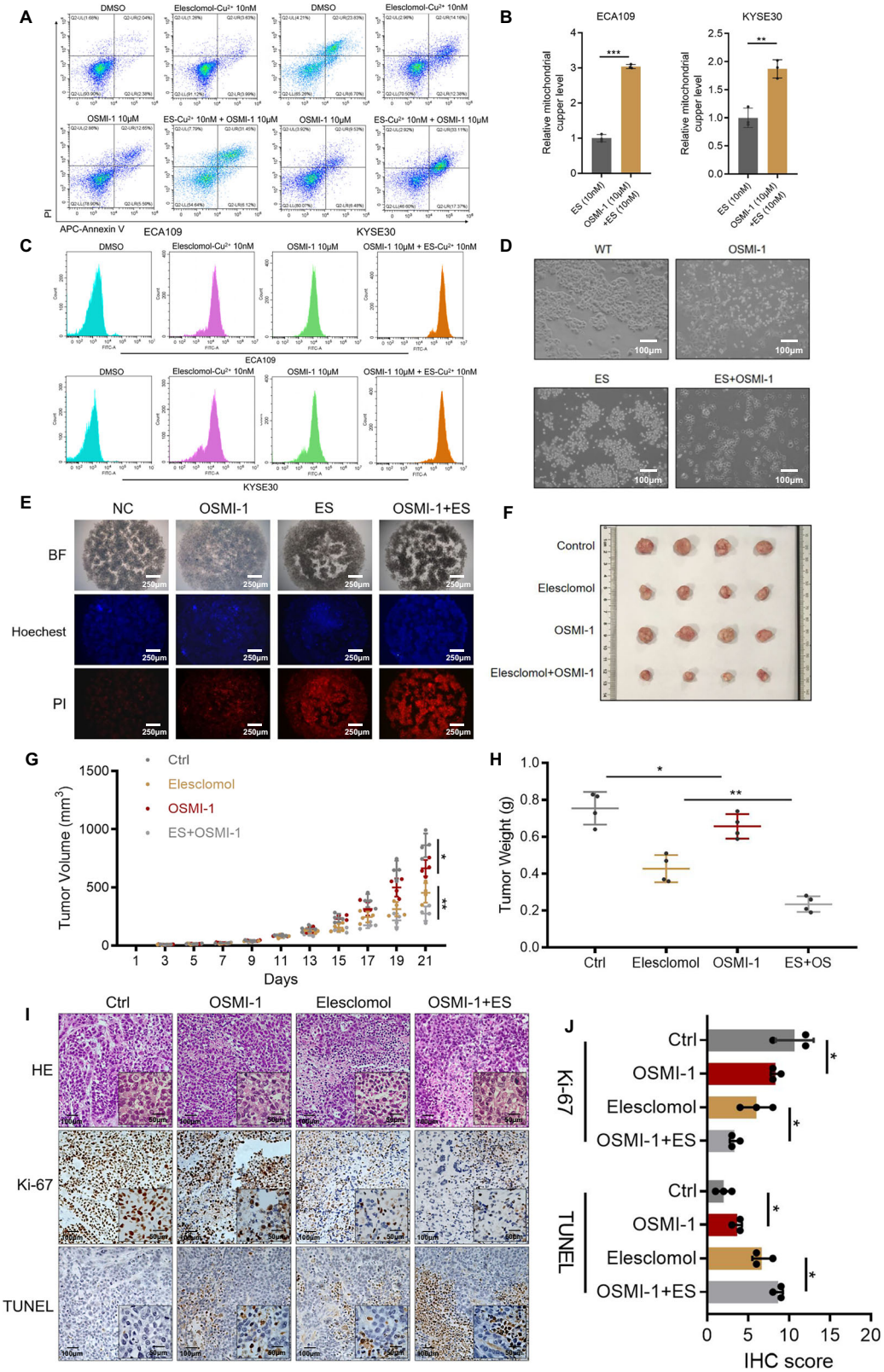

Fig. 6 | Combined application of Elesclomol and OSMI-1 significantly promotes cuproptosis. A Flow cytometry assessses cell apoptosis after treatment with OSMI-1 in combination with Elesclomol-Cu^{2+}. **B** The detection of mitochondrial copper ion concentration showed that OSMI-1 could increase the copper ion concentration in cellular mitochondria under ES-Cu^{2+} stimulation ($n = 3$ independent experiments). **C** Reactive oxygen species (ROS) detection revealed that OSMI-1 notably shifted the absorption peak to the right under Elesclomol-Cu^{2+} stimulation. **D** Morphological changes of ECA109 cells under different drug treatments were captured under a bright-field microscope. **E** 3D cell culture and staining with Hoechst and PI under different drug treatments. **F** Subcutaneous xenograft tumors in nude mice were established, with OSMI-1 or Elesclomol administered intraperitoneally ($n = 4$ independent experiments). **G** Tumor growth was depicted in the figure ($n = 4$ independent experiments). **H** Tumor weight was depicted in the figure ($n = 4$ independent experiments). **I** Immunohistochemical staining of Ki-67, TUNEL. **J** Quantification of I ($n = 4$ independent samples). Error bars indicate standard deviations (ns: none significant; *p<0.05; **p<0.01; ***p<0.001).

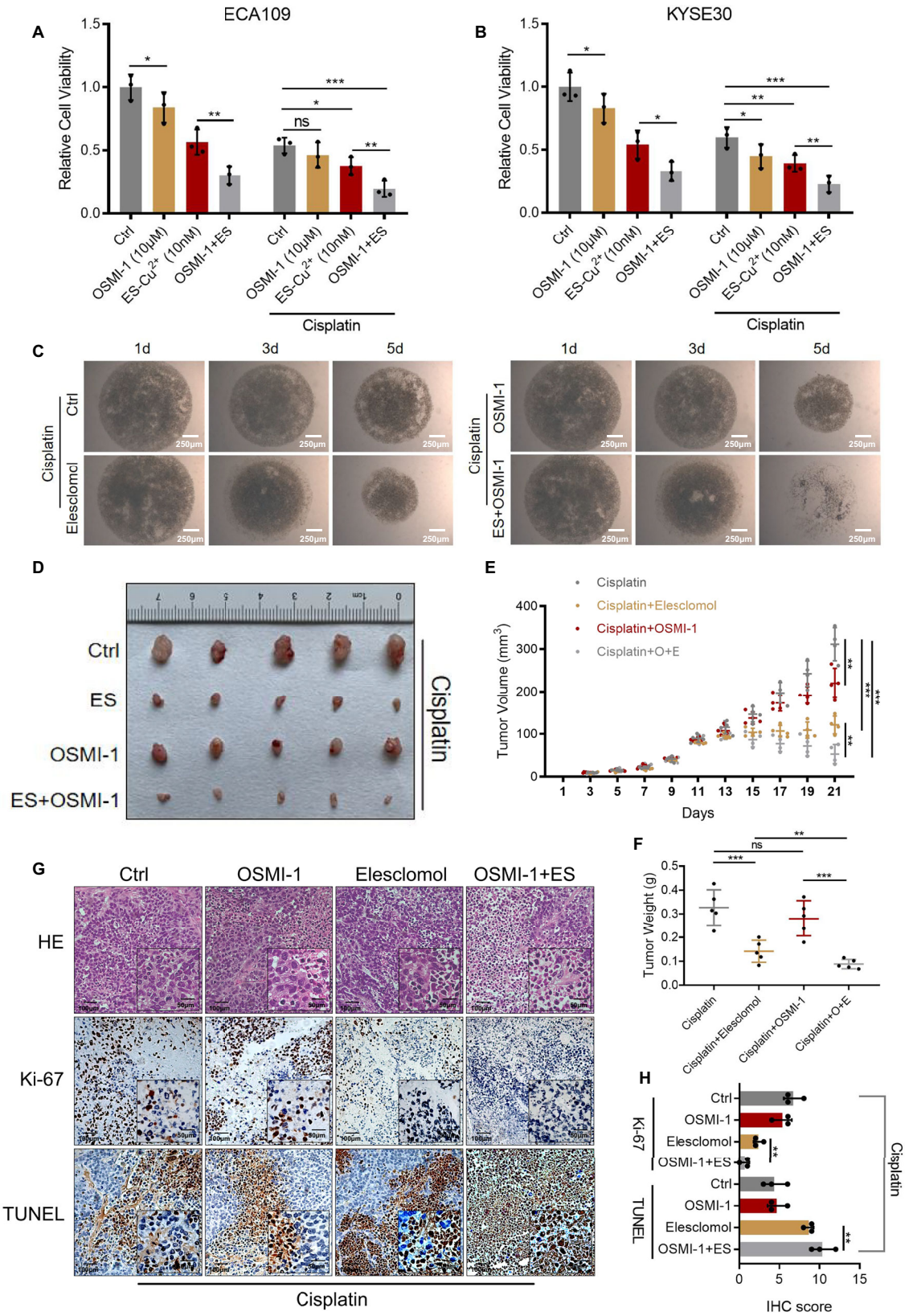

Fig. 7 | Sensitizing effects of OSMI-1 and Elesclomol on cisplatin. A Cell viability assays (CCK8) revealed near-complete inhibition of cell activity with the triple combination of OSMI-1, Elesclomol-Cu^{2+}, and cisplatin in ECA109 cell line ($n = 3$ independent experiments). **B** CCK8 assays of the same conditions with (**A**), in KYSE30 cell line ($n = 3$ independent experiments). **C** 3D cell culture experiments showed the combination of OSMI-1 and ES could significantly reduce or even eliminate 3D cell spheroids when combined with cisplatin. **D** Subcutaneous xenograft tumor in nude mice treated with indicated combinations of OSMI-1, Elesclomol-Cu^{2+}, and cisplatin ($n = 5$ independent experiments). **E** Tumor growth was depicted in the figure ($n = 5$ independent experiments). **F** Tumor weight was depicted in the figure ($n = 5$ independent experiments). **G** Immunohistochemical staining of Ki-67, TUNEL. **H** Quantification of (**G**) ($n = 3$ independent samples). Error bars indicate standard deviations (ns: none significant; $^{*}p < 0.05$; $^{**}p < 0.01$; $^{***}p < 0.001$).

After purification and fragmentation of the mRNA, these fragments were incubated with the primary antibody against m6A for immunoprecipitation using the Magna MeRIP™ m6A Kit (Merck Millipore, MA, USA). Subsequently, the enriched m6A-modified mRNA was detected by qRT-PCR.

Nuclear and cytoplasmic protein isolation

Whole-cell lysate (WCL) was extracted in 2% sodium dodecyl sulfate (SDS), 10% glycerol, 50 mM Tris pH 6.8, and 2 mM mercaptoethanol, boiled for 5–10 min, and loaded onto a gel immediately after cooling at room temperature. Nuclear and cytoplasmic proteins were extracted using the EpiQuik Nuclear Extraction Kit I (Epigentek) according to the manufacturer's instructions. Briefly, the cytoplasmic fraction was first removed from the nuclear pellet. Subsequently, 1% NP40, 50 mM Tris pH 8.0, 150 mM NaCl, 10% glycerol, and 1 mM EDTA were added to the nuclear pellet to extract nuclear proteins. The mixture was incubated on ice for 15 min with vortexing (5 s) every 3 min, followed by centrifugation at 14,000 rpm for 10 min at 4 °C. The nuclear and cytoplasmic fractions were then concentrated in Amicon Ultra Centrifugal Filters-10K (Millipore) for 5–15 min at 4 °C. Finally, 10% glycerol was added to the final cytoplasmic extract. All proteins were separated by SDS/polyacrylamide gel electrophoresis and transferred to a polyvinylidene fluoride (PVDF) membrane. Blocking was performed in 5% milk. The primary antibody was diluted according to the instructions. The PVDF membrane was incubated with the primary antibody overnight at 4 °C, followed by incubation with the secondary antibody for 1 h at room temperature. Imaging was performed using Millipore Immobilon Western Chemiluminescent HRP Substrate.

Mitochondrial copper measurement

For the measurement of mitochondrial copper, mitochondria were extracted from cultured cells using the mitochondria isolation kit (Thermo Scientific, 89874) according to the manufacturer's instructions. The isolated mitochondria were then digested in 2 mL of ultrapure concentrated nitric acid in closed PFA beakers on a hot plate at 150 °C overnight. After the concentrated nitric acid had evaporated, the samples were redissolved in 5 mL of 2% nitric acid. The resulting clear solutions were analyzed for copper content using ICP-MS (Agilent 8800 QQQ-ICP-MS)[47].

Statistics and reproducibility

All experiments were repeated at least three times, and the results are expressed as means ± SD. Student's t-test or the one-way ANOVA was used to analyze the data, and the χ^2-test was used to analyze differences in other variables, as appropriate. All statistical analyses were undertaken using GraphPad Prism software. A p value < 0.05 was considered statistically significant for all datasets ($^*p < 0.05$, $^{**}p < 0.01$, $^{***}p < 0.001$).

Ethics approval and consent to participate

Approval of the research protocol by an institutional review board: All procedures followed were in accordance with the ethical standards of the institutional review board of Tongji University School of Medicine with the Declaration of Helsinki 1964 and later versions. All ethical regulations relevant to human research participants were followed. All institutional and national guidelines for the care and use of laboratory animals were followed.

Reporting summary

Further information on research design is available in the Nature Portfolio Reporting Summary linked to this article.

Data availability

The expression of TRIM21 in ESCA was investigated in Ualcan Website (https://ualcan.path.uab.edu/analysis.html) based on TCGA database. The expression of TRIM21 in pan-cancer was analysed in TIMER2.0 Website (https://compbio.cn/timer2/) based on TCGA database. The expression of LIAS in ESCA and pan-cancer was analysed in Gepia website (http://gepia.cancer-pku.cn/detail.php?gene=LIAS) based on TCGA database. All uncropped original blots and raw data are included in the manuscript as Supplementary Information 9 (Supplementary Fig. 7) and Supplementary Information 10 (Supplementary Data 1). The raw mass spectrometry data can be referred to Integrated Proteome Resources (iProx[48,49], Project ID: IPX0014132000, dataset identifier PXD070439). The raw RNA sequence data reported in this paper have been deposited in the Sequence Read Archive (SRA) repository (Accession: PRJNA1357317). The datasets generated or analysed during the current study are available from the corresponding author on reasonable request.

Received: 2 April 2025; Accepted: 7 November 2025;
Published online: 18 December 2025

References

1. Sung, H. et al. Global cancer statistics 2020: GLOBOCAN estimates of incidence and mortality worldwide for 36 cancers in 185 countries. *CA Cancer J. Clin.* **71**, 209–249 (2021).
2. Smyth, E. C. et al. Oesophageal cancer. *Nat. Rev. Dis. Prim.* **3**, 17048 (2017).
3. Zhang, X. & Jain, D. Updates in staging and pathologic evaluation of esophageal carcinoma following neoadjuvant therapy. *Ann. N. Y Acad. Sci.* **1482**, 163–176 (2020).
4. Zhang, Y. et al. Outcomes of endoscopic submucosal dissection vs esophagectomy for T1 esophageal squamous cell carcinoma in a real-world cohort. *Clin. Gastroenterol. Hepatol.* **17**, 73–81.e3 (2019).
5. Ming, H. et al. Protein degradation: expanding the toolbox to restrain cancer drug resistance. *J. Hematol. Oncol.* **16**, 6 (2023).
6. Cai, C., Tang, Y. D., Zhai, J. & Zheng, C. The RING finger protein family in health and disease. *Signal Transduct. Target Ther.* **7**, 300 (2022).
7. Huang, N. et al. TRIM family contribute to tumorigenesis, cancer development, and drug resistance. *Exp. Hematol. Oncol.* **11**, 75 (2022).
8. Zhu, Z. M., Huo, F. C., Zhang, J., Shan, H. J. & Pei, D. S. Crosstalk between m6A modification and alternative splicing during cancer progression. *Clin. Transl. Med.* **13**, e1460 (2023).
9. Tang, B. et al. m(6)A demethylase ALKBH5 inhibits pancreatic cancer tumorigenesis by decreasing WIF-1 RNA methylation and mediating Wnt signaling. *Mol. Cancer* **19**, 3 (2020).
10. Li, B. et al. Surmounting cancer drug resistance: new insights from the perspective of N (6)-methyladenosine RNA modification. *Drug Resist. Updat.* **53**, 100720 (2020).
11. Chen, Y. et al. ALKBH5 suppresses malignancy of hepatocellular carcinoma via m(6)A-guided epigenetic inhibition of LYPD1. *Mol. Cancer* **19**, 123 (2020).
12. Wang, H. et al. ALKBH5 facilitates the progression of skin cutaneous melanoma via mediating ABCA1 demethylation and modulating autophagy in an m6A-dependent manner. *Int. J. Biol. Sci.* **20**, 1729–1743 (2024).
13. Zaccara, S., Ries, R. J. & Jaffrey, S. R. Reading, writing and erasing mRNA methylation. *Nat. Rev. Mol. Cell Biol.* **20**, 608–624 (2019).
14. Wedan, R. J., Longenecker, J. Z. & Nowinski, S. M. Mitochondrial fatty acid synthesis is an emergent central regulator of mammalian oxidative metabolism. *Cell Metab.* **36**, 36–47 (2024).
15. Cobine, P. A. & Brady, D. C. Cuproptosis: Cellular and molecular mechanisms underlying copper-induced cell death. *Mol. Cell* **82**, 1786–1787 (2022).
16. Wang, Y., Zhang, L. & Zhou, F. Cuproptosis: a new form of programmed cell death. *Cell Mol. Immunol.* **19**, 867–868 (2022).
17. Tang, D., Chen, X. & Kroemer, G. Cuproptosis: a copper-triggered modality of mitochondrial cell death. *Cell Res.* **32**, 417–418 (2022).
18. Nagai, M. et al. The oncology drug elesclomol selectively transports copper to the mitochondria to induce oxidative stress in cancer cells. *Free Radic. Biol. Med.* **52**, 2142–2150 (2012).

19. Zheng, P., Zhou, C., Lu, L., Liu, B. & Ding, Y. Elesclomol: a copper ionophore targeting mitochondrial metabolism for cancer therapy. *J. Exp. Clin. Cancer Res.* **41**, 271 (2022).
20. Yan, J. N. et al. Clinical significance and potential application of cuproptosis-related genes in gastric cancer. *World J. Gastrointest. Oncol.* **15**, 1200–1214 (2023).
21. Shi, B., Zhang, W., Wang, T. & Cui, Z. The therapeutic and prognostic role of cuproptosis-related genes in triple negative breast cancer. *BMC Bioinforma.* **24**, 223 (2023).
22. Jiang, X. et al. A novel cuproptosis-related gene signature of prognosis and immune microenvironment in head and neck squamous cell carcinoma cancer. *J. Cancer Res Clin. Oncol.* **149**, 203–218 (2023).
23. Lin, A. P. et al. MYC, mitochondrial metabolism and O-GlcNAcylation converge to modulate the activity and subcellular localization of DNA and RNA demethylases. *Leukemia* **36**, 1150–1159 (2022).
24. Wang, H. et al. The OGT-c-Myc-PDK2 axis rewires the TCA cycle and promotes colorectal tumor growth. *Cell Death Differ*. https://doi.org/10.1038/s41418-024-01315-4 (2024).
25. Yang, Y. et al. O-GlcNAcylation of YTHDF2 promotes HBV-related hepatocellular carcinoma progression in an N6-methyladenosine-dependent manner. *Signal Transduct. Target Ther.* **8**, 63 (2023).
26. Wangpaichitr, M. et al. N',N'-Dimethyl-N',N'-bis(phenylcarbonothioyl) propanedihydrazide (elesclomol) selectively kills cisplatin resistant lung cancer cells through reactive oxygen species (ROS). *Cancers.* **1**, 23–38 (2009).
27. Li, J. Y. et al. TRIM21 inhibits irradiation-induced mitochondrial DNA release and impairs antitumour immunity in nasopharyngeal carcinoma tumour models. *Nat. Commun.* **14**, 865 (2023).
28. Alomari, M. TRIM21—a potential novel therapeutic target in cancer. *Pharm. Res.* **165**, 105443 (2021).
29. Wan, S. et al. SPARC stabilizes ApoE to induce cholesterol-dependent invasion and sorafenib resistance in hepatocellular carcinoma. *Cancer Res.* **84**, 1872–1888 (2024).
30. Ye, W. L. et al. TRIM21 induces selective autophagic degradation of c-Myc and sensitizes regorafenib therapy in colorectal cancer. *Proc. Natl. Acad. Sci. USA* **121**, e2406936121 (2024).
31. Liu, Y. X. et al. TRIM21 is a druggable target for the treatment of metastatic colorectal cancer through ubiquitination and activation of MST2. Cell. *Chem. Biol.* **30**, 709–725.e6 (2023).
32. Qu, J. et al. RNA demethylase ALKBH5 in cancer: from mechanisms to therapeutic potential. *J. Hematol. Oncol.* **15**, 8 (2022).
33. Tsvetkov, P. et al. Copper induces cell death by targeting lipoylated TCA cycle proteins. *Science* **375**, 1254–1261 (2022). Erratum in: *Science* 376, eabq4855 (2022).
34. Xie, J., Yang, Y., Gao, Y. & He, J. Cuproptosis: mechanisms and links with cancers. *Mol. Cancer* **22**, 46 (2023).
35. Babu, A., Fernandez, A., Viswanadhan Sarasamma, V. & Pathumma Laila, S. Synthesis and characterisation of copper acetate mediated oxidative coupled product of naturally occurring hydroxy benzoquinone, embelin and its in vitro and in vivo cytotoxic studies in Dalton Lymphoma ascites tumour cells. *Nat. Prod. Res.* **39**, 1039–1049 (2025).
36. Sun, L. et al. Lactylation of METTL16 promotes cuproptosis via m(6)A-modification on FDX1 mRNA in gastric cancer. *Nat. Commun.* **14**, 6523 (2023).
37. Li, S. R., Bu, L. L. & Cai, L. Cuproptosis: lipoylated TCA cycle proteins-mediated novel cell death pathway. *Signal Transduct. Target Ther.* **7**, 158 (2022).
38. Chang, G. et al. USP36 promotes tumorigenesis and drug sensitivity of glioblastoma by deubiquitinating and stabilizing ALKBH5. *Neuro Oncol.* **25**, 841–853 (2023). Erratum in: *Neuro Oncol.* 25, 1913 (2023).
39. Yu, F. et al. Post-translational modification of RNA m6A demethylase ALKBH5 regulates ROS-induced DNA damage response. *Nucleic Acids Res.* **49**, 5779–5797 (2021).
40. Liu, M. et al. Macrophage K63-linked ubiquitination of YAP promotes its nuclear localization and exacerbates atherosclerosis. *Cell Rep.* **32**, 107990 (2020).
41. Li, T. et al. O-GlcNAc transferase links glucose metabolism to MAVS-mediated antiviral innate immunity. *Cell Host Microbe* **24**, 791–803.e6 (2018).
42. Wang, X. et al. O-GlcNAcylation modulates HBV replication through regulating cellular autophagy at multiple levels. *FASEB J.* **34**, 14473–14489 (2020).
43. Wang, Y. et al. Cuproptosis: a novel therapeutic target for overcoming cancer drug resistance. *Drug Resist Updat* **72**, 101018 (2024).
44. Sun, L. et al. Lactylation of METTL16 promotes cuproptosis via m6A-modification on FDX1 mRNA in gastric cancer. *Nat. Commun.* **14**, 6523 (2023).
45. Li, H. et al. ZIP10 drives osteosarcoma proliferation and chemoresistance through ITGA10-mediated activation of the PI3K/AKT pathway. *J. Exp. Clin. Cancer Res.* **40**, 340 (2021).
46. Feng, A., He, L., Chen, T. & Xu, M. A novel cuproptosis-related lncRNA nomogram to improve the prognosis prediction of gastric cancer. *Front Oncol.* **12**, 957966 (2022).
47. Lei, G. et al. Radiotherapy promotes cuproptosis and synergizes with cuproptosis inducers to overcome tumor radioresistance. *Cancer Cell.* **43**, 1076–1092.e5 (2025).
48. Ma, J. et al. iProX: an integrated proteome resource. *Nucleic Acids Res.* **47**, D1211–D1217 (2019).
49. Chen, T. et al. iProX in 2021: connecting proteomics data sharing with big data. *Nucleic Acids Res.* **50**, D1522–D1527 (2022).

Acknowledgements

This work was supported by grants from National Natural Science Foundation of China [82072684 (M.D.X.), 82073224 (T.C.), and 82372921 (T.C.)]; the Medical Discipline Construction Project of Pudong Health Committee of Shanghai [PWZxq2022-6 (M.D.X.)], and Outstanding Young Medical Talents and Outstanding Projects of Shanghai Municipal Health Commission [20224Z0016 (T.C.)], and the Fundamental Research Funds for the Central Universities [22120240372 (T.C.)], National Natural Science Foundation of China [82203341 (L.N.H.)], The Fundamental Research Funds for the Central Universities [22120240371 (L.N.H.)], the Excellent Young Medical Talent Development Program in Pudong New Area Health System [PWRq2024-10 (L.N.H.)]. We thank Professor. Guohan Chen (Shanghai East Hospital, Tongji University School of Medicine, Shanghai, China) for assistance with sample collection.

Author contributions

M.D.X. and T.C. conceived and designed the study. A.Q.F., L.N.H., and Z.X.L. conducted most of the experiments. Z.H.Z., K.F., H.W., and Z.Y.Z. helped in some experiments. A.Q.F. and L.N.H. wrote the original draft of the manuscript. M.D.X., T.C., and L.N.H. contributed to draft revising and funding. L.Z., A.Q.F., X.Y.W., and L.N.H. contributed to sample collection and data analysis. M.C.S., Z.Y.W., Z.K.C., and S.H.Z. participated in methodology supervision and draft revising. All authors contributed to the article and approved the submitted version.

Competing interests

The authors declare no competing interests.

Consent for publication

All authors are in agreement with the content of the manuscript and consent for publication.

Informed consent

All human samples were obtained with the patients' written informed consent and consent to publish information that identifies individuals has been obtained.

Additional information

Supplementary information The online version contains supplementary material available at https://doi.org/10.1038/s42003-025-09201-6.

Correspondence and requests for materials should be addressed to Tao Chen or Meidong Xu.

Peer review information *Communications Biology* thanks Hua Wu, Jian Wu and the other, anonymous, reviewer(s) for their contribution to the peer review of this work. Primary Handling Editors: Manuel Breuer and Johannes Stortz.

Reprints and permissions information is available at http://www.nature.com/reprints

Publisher's note Springer Nature remains neutral with regard to jurisdictional claims in published maps and institutional affiliations.

Open Access This article is licensed under a Creative Commons Attribution-NonCommercial-NoDerivatives 4.0 International License, which permits any non-commercial use, sharing, distribution and reproduction in any medium or format, as long as you give appropriate credit to the original author(s) and the source, provide a link to the Creative Commons licence, and indicate if you modified the licensed material. You do not have permission under this licence to share adapted material derived from this article or parts of it. The images or other third party material in this article are included in the article's Creative Commons licence, unless indicated otherwise in a credit line to the material. If material is not included in the article's Creative Commons licence and your intended use is not permitted by statutory regulation or exceeds the permitted use, you will need to obtain permission directly from the copyright holder. To view a copy of this licence, visit http://creativecommons.org/licenses/by-nc-nd/4.0/.

© The Author(s) 2025